7674 *Biochemistry* **2010,** *49,* 7674–7682
DOI: 10.1021/bi100973m

BIOCHEMISTRY
including biophysical chemistry & molecular biology
Article

Identification of a Regulatory Segment of Poly(ADP-ribose) Glycohydrolase[†]

Davide Botta and Myron K. Jacobson*

Department of Pharmacology and Toxicology, College of Pharmacy and Arizona Cancer Center, University of Arizona, Tucson, Arizona 85724

Received June 16, 2010; Revised Manuscript Received August 3, 2010

ABSTRACT: Coordinate regulation of PARP-1 and -2 and PARG is required for cellular responses to genotoxic stress. While PARP-1 and -2 are regulated by DNA breaks and covalent modifications, mechanisms of PARG regulation are poorly understood. We report here discovery of a PARG regulatory segment far removed linearly from residues involved in catalysis. Expression and analysis of human PARG segments identified a minimal catalytically active C-terminal PARG (hPARG59) containing a 16-residue N-terminal mitochondrial targeting sequence (MTS). Deletion analysis and site-directed mutagenesis revealed that the MTS, specifically hydrophobic residues L473 and L474, was required for PARG activity. This region of PARG was termed the "regulatory segment/MTS" (REG/MTS). The overall α-helical composition of hPARG59, determined by circular dichroism (CD), was unaffected by mutation of the REG/MTS leucine residues, suggesting that activity loss was not due to incorrect protein folding. REG/MTS was predicted to be in a loop conformation because the CD spectra of mutant Δ1−16 lacking the REG/MTS showed a higher α-helical content than hPARG59, indicating a secondary structure other than α-helix for this segment. Deletion of the REG/MTS from full-length hPARG111 also resulted in a complete loss of activity, indicating that all PARG isoforms are subject to regulation at this site. The presence of the REG/MTS raises the possibility that PARG activity is regulated by interactions of PARP-1 and -2 and other proteins at this site, raises interesting questions concerning mitochondrial PARG because MTS residues are often removed after transport, and offers a potentially novel site for drug targeting of PARG.

The synthesis of polymers of ADP-ribose (PAR)[1] is an immediate cellular response to DNA strand breaks caused by oxidative stress, ionizing radiation, or alkylating agents (*1*−*3*). A primary enzyme involved in this post-translational modification is poly(ADP-ribose) polymerase-1 (PARP-1), which belongs to a growing family of PARPs that includes a second member (PARP-2) that also responds to DNA strand breaks (*4*, *5*). Upon binding to DNA strand breaks, PARP-1 and -2 use nicotinamide adenine dinucleotide (NAD^+) as a substrate to synthesize PAR targeted to the PARPs themselves and other nuclear acceptor proteins, such as histones, p53, and enzymes involved in DNA repair (*6*). PARP-1 is inactivated and released from the DNA strand break by its automodification. Poly(ADP-ribose) glycohydrolase (PARG) is the endoexoglycohydrolase that catalyzes PAR turnover via the hydrolysis of the α(1″ → 2′) and α(1‴ → 2″) ribosyl−ribose linkages to produce free ADP-ribose (ADPR) (*7*).

Unlike the PARPs that are encoded by multiple genes, only a single PARG gene with a clearly defined function in PAR hydrolysis has been detected in mammals (*8*). A structurally unrelated 39 kDa enzyme exhibiting PARG activity has been identified and characterized (*9*), but its functional significance remains to be elucidated. The PARG gene encodes a full-length 111 kDa PARG protein (hPARG111) that localizes to the nucleus, but several other PARG isoforms are expressed in different cell compartments from alternative splice variants of the human *PARG* RNA transcripts (*10*, *11*). These include hPARG102 and hPARG99, which lack the N-terminal nuclear localization signal (NLS) coded by exon 1 and show an extranuclear localization (*10*), and a hPARG59 isoform that localizes to the mitochondria (*11*, *12*).

Several significant strides in understanding the structural and functional relationship of PARG have been made in the past decade. Deletion of the PARG gene results in a complete loss of cellular PARG activity and early embryonic lethality of homozygous mutant mice (*13*), suggesting that there are no significant compensatory mechanisms for the catabolism of PAR. Partial deletion of the PARG gene in both *Drosophila melanogaster* (*14*) and mice (*13*, *15*) sensitizes cells to DNA damage induced by alkylating agents and ionizing radiation. Upon genotoxic stress, both PARP-$1^{-/-}$ mouse embryonic fibroblasts (MEF) (*16*) and cells derived from a hypomorphic mutant mouse model in which exons 2 and 3 of PARG were deleted (PARG-Δ2,3) (*17*) showed a reduced level of formation of XRCC1 foci, indicating that the regulation of PAR levels is achieved via a precise coordination of PARP and PARG activities critical for normal cellular responses to DNA damage.

[†]Supported by Grant CA 43894 from the National Institutes of Health to M.K.J.

*To whom correspondence should be addressed: Arizona Cancer Center, Room 3985, University of Arizona, 1515 N. Campbell Ave., Tucson, AZ 85724. Telephone: (520) 626-5957. Fax: (520) 626-8657. E-mail: mjacobson@pharmacy.arizona.edu.

[1]Abbreviations: PAR, poly(ADP-ribose); PARG, poly(ADP-ribose) glycohydrolase; hPARG, human PARG; PARP-1 and -2, poly(ADP-ribose) polymerases 1 and 2, respectively; ADPR, ADP-ribose; ADPRT, ADP-ribosyltransferase; NAD^+, nicotinamide adenine dinucleotide; MTS, mitochondrial targeting sequence; CD, circular dichroism; MEF, mouse embryonic fibroblasts; XRCC1, X-ray repair cross complementing group 1; PCR, polymerase chain reaction; TEV, tobacco etch virus; PMSF, phenylmethanesulfonyl fluoride; Ni-NTA, nickel-nitrilotriacetic acid; MBP, maltose binding protein; BSA, bovine serum albumin; TLC, thin layer chromatography; SDS, sodium dodecyl sulfate; MPP, mitochondrial processing peptidase; SSL, synthetic sickness/lethality.

 Published on Web 08/04/2010

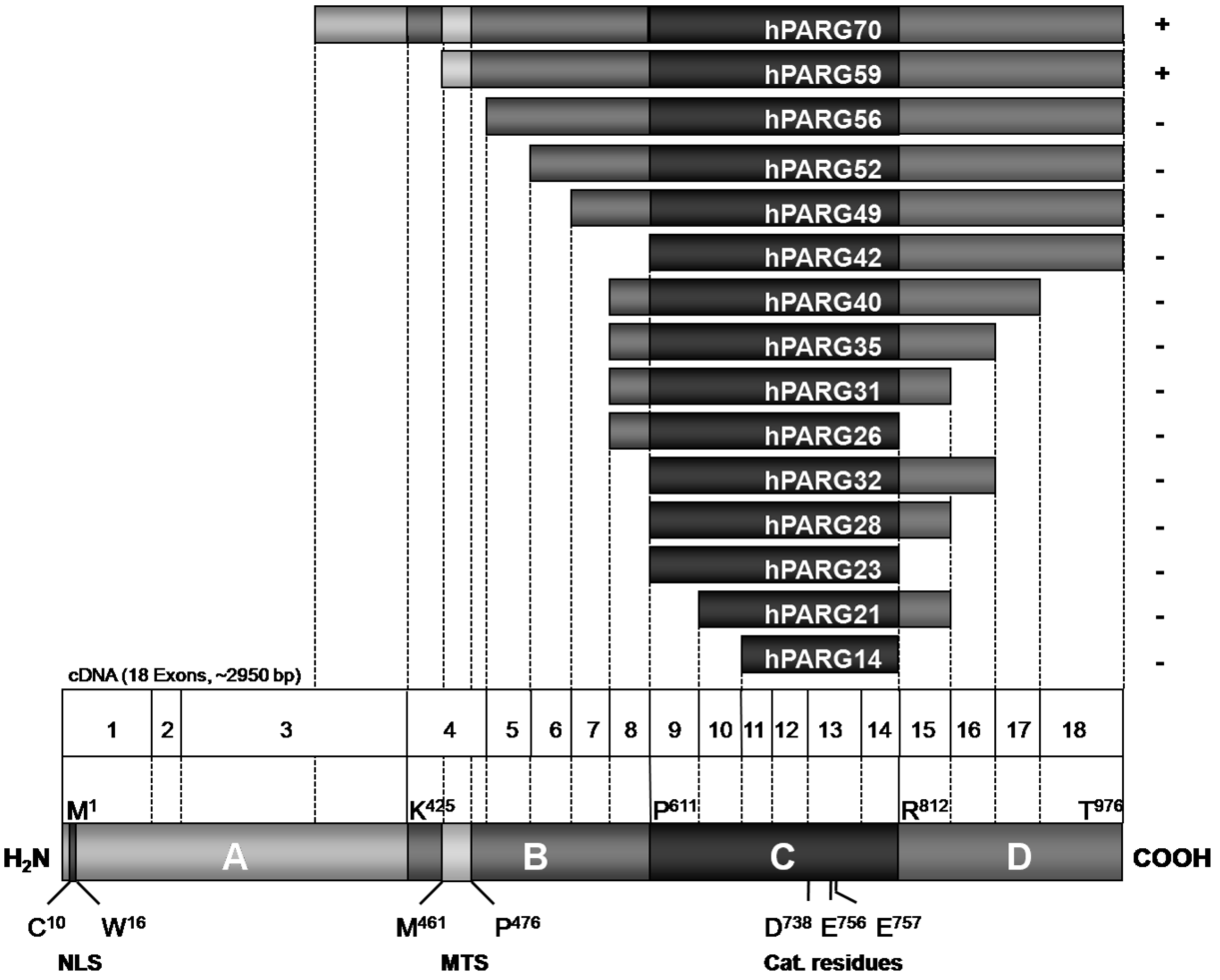

FIGURE 1: Determination of the minimal catalytically active PARG. The 15 PARG fragments synthesized and tested for enzymatic activity are shown in relation to the full-length hPARG111 protein. Each fragment is labeled according to its size in kilodaltons and is indicated on the right as being either catalytically active (+) or inactive (−).

An inhibitor binding site of PARG, T796, was recently identified (*18*) and found to be in a highly conserved region of the protein coded by exons 13 and 14, which also contains three catalytically essential acidic residues (D738, E756 and E757) (*19*), and a glycine-rich region (G745-G746-G747) (*20*) important for PARG function. These findings allowed a "signature sequence" to be defined and led to the putative assignment of a domain structure for PARG (Figure 1) (*19*, *21*).

Extensive work on PARP-1 has led to the discovery of several different mechanisms of regulation for this enzyme. Two N-terminal zinc finger domains in PARP-1 have been shown to bind to various DNA structures (*22*) and thereby activate the catalytic domain situated at the C-termini of the enzymes. Recently, a third zinc-binding domain has been identified in human PARP-1, and it has been shown to be essential for the DNA-dependent activity (*23*) as well as the chromatin compaction activity of the enzyme (*24*). Both PARP-1 activation following DNA damage (*25*) and DNA damage-independent PARP-1 activation (*26*) were found to be dependent on phosphorylation by activated extracellular signal-regulated kinases 1 and 2 (*25*), and the role of PARP-1 in transcriptional regulation was found to be regulated by acetylation of specific lysine residues (*27*). In spite of our improving understanding of PARP-1 regulation, to date no information about how PARG is regulated is available. We report here structure−function studies that have led to the discovery of the first potential mechanism of regulation of PARG via the identification of amino acid residues required for PARG activity that are far removed from the putative catalytic domain of the enzyme. Intriguingly, these residues are located within a 16-residue mitochondrial targeting sequence (MTS) of the enzyme.

MATERIALS AND METHODS

Materials. The pMAL-c2x and pBAD102/D-TOPO parent vectors were purchased from New England Biolabs (Ipswich, MA) and Invitrogen (Carlsbad, CA), respectively. [α-^{32}P]NAD$^+$ used for the synthesis of radiolabeled PAR was purchased from Perkin-Elmer (Waltham, MA).

Synthesis and Cloning of PARG Fragments and Mutants. Primers were designed to produce polymerase chain reaction (PCR) products with the ENLYFQ/S tobacco etch virus (TEV) protease cleavage site coding sequence preceding each PARG fragment and mutant, and with SalI and PmeI restriction sites at the 5′ and 3′ ends, respectively. The PARG mutants were synthesized with the use of previously constructed and reported mutant PARG plasmids as templates for the PCR (*12*). Each PCR product was cloned into a dual hexahistidine-maltose binding protein (His_6-MBP) fusion protein expression vector pMAL-His_6-malE, a modified pMAL-c2x expression vector (New England Biolabs) in which hexahistidine coding bases were inserted at the 5′ end of the malE gene that encodes the MBP tag (Figure 2A). Plasmids were amplified in electrocompetent *Escherichia coli* TOP10 (Invitrogen), isolated using the QIAprep Spin Miniprep

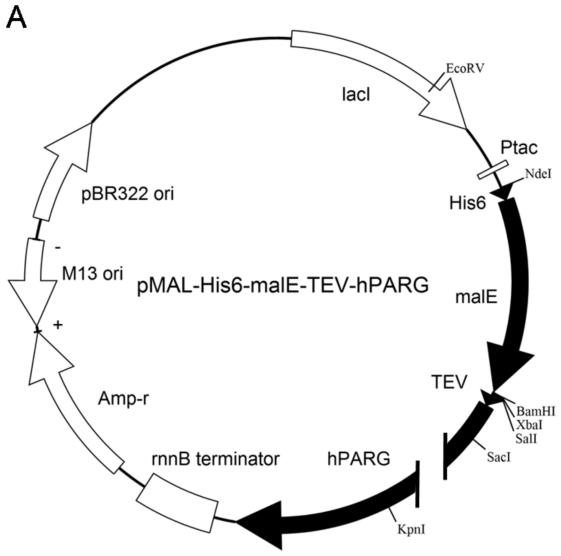

C

Protein	K_M (μM)	V_{MAX} (nmol/min/mg)
Uncleaved hPARG59	1.86 ± 0.75	0.9 ± 0.1
Cleaved hPARG59	2.80 ± 0.83	1.1 ± 0.2

FIGURE 2: Preparation of PARG fragments and mutants. (A) Bacterial expression plasmid pMAL-His_6-malE-TEV-hPARG used for the expression of the PARG fragments and mutants discussed in this study. (B) Coomassie blue staining of the Ni^{2+}-purified hPARG59 fragment before (lane 1) and after (lane 2) removal of the His_6-MBP dual tag by TEV. The bands present following cleavage are the uncleaved fusion protein His_6-MBP-TEV-hPARG59 (103 kDa, band a), the cleaved hPARG59 protein (59 kDa, band b), the Pro-TEV protease (50 kDa, band c), the truncated TEV autoproteolysis product (47 kDa, band d), and the cleaved His_6-MBP tag (43 kDa, band e). (C) Enzyme kinetic parameters of bacterially expressed hPARG59 before and after cleavage of the His_6-MBP fusion tag. The K_m and V_{max} values and standard errors were determined using GraphPad Prism and are expressed as mean values of a representative experiment conducted in triplicate.

kit (Qiagen), and sequenced to ensure correct orientation of the PARG inserts.

Deletion Mutations of the MTS. The QuikChange II XL site-directed mutagenesis kit (Stratagene) was used, following the manufacturer's protocol, to obtain a deletion mutation of residues 461−476 in the full-length hPARG111 protein. Briefly, pBAD102/D-TOPO-hPARG111, a large expression vector containing the full-length protein, was amplified in its entirety by PCR using the PfuUltra High-Fidelity DNA polymerase and deletion primers hP111-Δ461−476for (5′-GGC TTG GAA CTC CCA TTG AGG AGT CTG CCA ATC ACA CAG TAA CTA TTC GG-3′) and hP111-Δ461−476rev (5′-CCG AAT AGT TAC TGT GTG ATT GGC AGA CTC CTC AAT GGG AGT TCC AAG CC-3′). The amplification reaction product was treated with the restriction enzyme DpnI for the digestion of parental methylated and hemimethylated DNA and then transformed into XL10-Gold ultracompetent cells for amplification.

Expression and Purification of PARG Fragments and Mutants. The pMAL-His_6-malE-TEV-hPARG plasmids were transformed into the electrocompetent *E. coli* K12 TB1 strain (New England Biolabs) by electroporation. Cells were grown in 500 mL of Rich medium (10 g/L bactotryptone, 5 g/L yeast extract, 5 g/L NaCl, and 2 g/L D-glucose) containing 100 μg/mL ampicillin until the A_{600} reached 0.5−0.6. Expression was induced by the addition of IPTG to a final concentration of 0.3 mM. Cells were then grown for an additional 2 h at 37 °C, harvested by centrifugation, and stored at −80 °C. The pBAD102/D-TOPO-hPARG plasmids were instead transformed into the electrocompetent *E. coli* Rosetta strain (Novagen), grown in LB medium, and expressed for 4 h using 0.2% L-arabinose. Thawed cells were resuspended in lysis buffer [50 mM potassium phosphate buffer (pH 7.5), 300 mM KCl, 50 mM imidazole, 10% glycerol, 0.1% Triton X-100, 1 mM PMSF, 1 mg/mL aprotonin, 1 mg/mL leupeptin, and 1 mg/mL pepstatin A] and subjected to sonification to rupture the cell membrane. After a 30 min centrifugation at 10000 rpm, the supernatant was loaded onto a 0.5 mL Ni-NTA agarose column (Invitrogen) and allowed to pass through by gravity flow. The column was washed twice with 5 mL of wash buffer (similar to the lysis buffer but lacking the protease inhibitors), and the protein was eluted with 1.5 mL of elution buffer [50 mM potassium phosphate buffer (pH 7.5), 300 mM KCl, 100 mM imidazole, 10% glycerol, 0.1% Triton X-100, and 1 mM maltose]. Following addition of 40 units of HQ-tagged TEV (Promega) to 40 μg of purified protein, the cleavage reaction was conducted in elution buffer for 16 h at 4 °C.

PARG Activity Assay. This assay utilizes conditions previously reported (*28*). Briefly, a typical reaction mixture was prepared via addition of 5 μL of 3× glyco assay buffer [150 mM potassium phosphate buffer (pH 7.5), 150 mM KCl, 0.3 mg/mL BSA, and 30 mM 2-mercaptoethanol], 2.5 μL of 60 μM [α-^{32}P]PAR (approximately 6000 cpm/μL), and 5 μL of deionized water. A total of 2.5 μL of each TEV cleavage reaction product was added, and the reaction mixtures were incubated at 37 °C for 10−60 min. The reactions were then stopped by the addition of 2 μL of 1% SDS. Next, 3 μL of each reaction mixture was loaded onto a 2 cm × 10 cm poly(ethyleneimine)-cellulose F TLC plate, prespotted with 1 μL of 40 mM ADP-ribose. The spots were dried, and the plates were placed into a TLC tank with 100 mL of methanol and developed until the solvent front reached the top of the plate. The plates were then transferred into a second tank containing 100 mL of a 0.9 M/0.3 M acetic acid/LiCl solution. Once developed, the plates were air-dried, and the origins (containing PAR) and ADPR spots (visible under a short-wave UV lamp) were excised and placed into separate 20 mL scintillation vials containing 10 mL of EcoLume. The radioactivity was counted in a Beckman liquid scintillation counter.

Circular Dichroism (CD) Spectrophotometry. CD spectra were recorded in the wavelength range of 200−260 nm with an Olis DSM20 spectropolarimeter (Jasco, Easton, MD) using a 0.1 cm

path length stain-free cell. The fusion proteins were analyzed at a concentration of 0.3 mg/mL in 5 mM KH_2PO_4 (pH 7.5), 25 mM KCl, and 1% glycerol at 20 °C. Spectra were recorded in millidegrees of ellipticity (θ). The solvent spectrum was subtracted from the sample spectra, and three independent measurements were used to calculate the mean residue ellipticity, [θ], using the formula

$$[\theta] = (100\theta)/(cln)$$

where [θ] is the mean residue ellipticity in degrees square centimeters per decimole, θ is the experimental ellipticity in millidegrees, c is the protein concentration in millimolarity, l is the cell path length in centimeters, and n is the number of residues in the protein (*29*). Assuming that the mean residue ellipticity at 222 nm is exclusively due to the α-helix conformation, fractional helicities were calculated using the following equation:

$$\% \text{ helicity} = [([\theta]_{222} + 2340 \text{ deg cm}^2 \text{ dmol}^{-1}) / (30300 \text{ deg cm}^2\text{dmol}^{-1})] \times 100$$

where $[\theta]_{222}$ is the observed mean residue ellipticity at 222 nm and 2340 and 30300 deg cm^2 $dmol^{-1}$ are previously determined values corresponding to 0 and 100% helix content at 222 nm, respectively (*30*).

Secondary Structure Predictions. The secondary structures of PARP-1, PARP-2, and PARG were predicted by submitting primary sequences to the online PredictProtein server (*31*). The reported results were obtained with the PHD (EMBL-Heidelberg) (*32*) and $PROF_{sec}$ (Profile network prediction Heidelberg) (*33*) algorithms. $PROF_{sec}$ is currently one of the most reliable profile-based neuronal network systems for predicting secondary structures of proteins with a three state per residue accuracy of 76% (*34*). MTS predictions were made using the MitoProtII computational method (*35*).

RESULTS

The Minimal Catalytically Active PARG Is a 59 kDa C-Terminal Fragment. Previous work by our laboratory identified a highly conserved inhibitor-binding residue of PARG, T796 (*18*), as well as three essential catalytic residues, D738, E756, and E757 (*19*), all localized in a region of the putative domain C encoded by exons 12 and 13 of the human PARG gene. These findings, together with the functional characterization of a glycine-rich segment, G745-G746-G747 (*20*), also present in this region of PARG, allowed for the definition of a "PARG signature" sequence that suggested that putative domain C represented the minimal catalytic domain of PARG. To test this hypothesis, 15 different fragments of human PARG cDNA were cloned into a His_6-MBP fusion protein expression vector as described in Materials and Methods. Each PARG fragment was expressed, purified by affinity chromatography, cleaved using TEV protease, and tested for PARG activity. The PARG assay used in this study measures the release of free ADP-ribose, thus measuring the exoglycosidase activity of PARG, which represents the major activity of the enzyme. Analysis of each PARG fragment was achieved via SDS−PAGE and Coomassie Blue Staining to confirm expression, purity, and TEV cleavage efficiency prior to catalytic activity determination. Figure 2B shows the high degree of purity (lane 1) and efficient TEV cleavage (lane 2) of hPARG59, one of the larger fragments tested, as an example of the purity verification. Michaelis−Menten kinetic analyses performed on hPARG59 showed that the K_m and V_{max} values for this fragment prior to and after removal of the His_6-MBP tag were similar (Figure 2C), indicating that the 45 kDa His_6-MBP dual tag did not exert a significant effect on PARG activity. For these experiments, activity of both cleaved and uncleaved proteins was examined. The fragments were designed so that they included the active site residues encoded by exons 12 and 13 and varied in the number of exon-encoded residues included on either side of the active site region (Figure 1). The designation of each fragment corresponds to its size in kilodaltons. Unexpectedly, only the largest two fragments, hPARG70 and hPARG59, demonstrated enzymatic activity. Similar results were observed with the corresponding uncleaved fusion proteins (data not shown).

The results in Figure 1 identified hPARG59 as the minimal catalytically active protein among the fragments analyzed. We were particularly intrigued by the lack of enzymatic activity of hPARG56, a fragment that differs from the active hPARG59 only by its lack of 26 residues encoded by exon 4, which contain a recently detected 16-residue N-terminal MTS (*11*, *12*).

Deletion of the PARG MTS Results in the Complete Loss of Catalytic Activity. To assess the role of the 16-residue MTS in the catalytic activity of PARG, four different deletion mutants were constructed (Figure 3). Each mutant was expressed, purified, cleaved with TEV, and tested for activity as described in Materials and Methods. The specific activity of each protein was measured using results from two separate experiments, each analyzed in triplicate assays. The activity of the deletion mutants was compared to that of the active minimal catalytic fragment, hPARG59, which possesses the full MTS. The deletion of the first four residues of the MTS, namely, M1, R2, R3, and M4 (mutant Δ1−4), resulted in an approximately 70% decrease in catalytic activity compared to that of hPARG59. As the deletion progressed toward the C-terminal end of the MTS, the activity decreased to a minimum where the deletion of residues M1−P12 (mutant Δ1−12) as well as the entire MTS (mutant Δ1−16) resulted in no detectable activity. These results indicate that the amino acids present in the MTS of PARG are required for the activity of the enzyme.

Adjacent Hydrophobic Residues L13 and L14 in the C-Terminal Half of the MTS Are Essential for PARG Function. A general feature of many MTS is an amphipathic α-helix (*11*, *36*). Despite a lack of primary sequence homology, MTS are generally highly basic, contain no acidic residues, and have a high percentage of leucine, serine, and arginine residues. To determine which residues are essential for PARG activity, the MTS was interrogated by site-directed mutagenesis. The basic arginine residues at positions 2, 3, 6, and 10 were mutated to hydrophobic alanine residues to reduce the net positive charge of the MTS, and the hydrophobic leucine residues at positions 11, 13, and 14 were mutated to acidic aspartate residues to disturb the hydrophobic region of the MTS while retaining a similar side chain size. Figure 3 shows the mutants constructed and the effect on PARG activity. The R2A mutation alone was the only arginine mutation to result in a significant loss of PARG activity, which was ~50% of that of wild-type hPARG59. The R3A and combined R2A/R3A/R6A/R10A mutations had no significant effect on PARG activity, while the R6A and R10A mutations resulted in a significant increase in activity. The L11D mutation alone did not decrease PARG activity. However, the double L11D/L13D mutant almost entirely abolished it, and the triple L11D/L13D/L14D mutant resulted in no detectable activity. These findings complement the deletion mutation results by identifying a regulatory segment in the MTS region of PARG. Specifically,

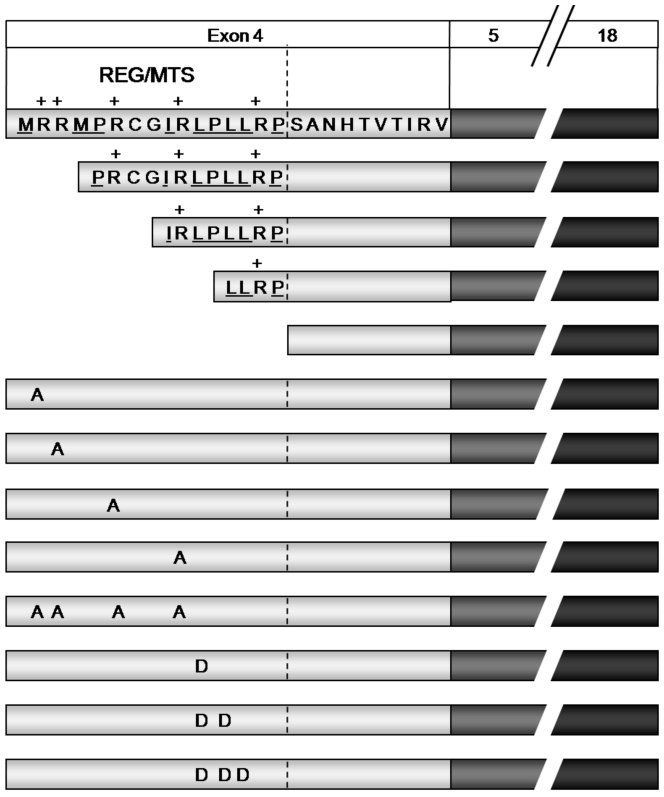

Protein	Specific Activity (nmol/min/mg)	Activity (%)
hPARG59	0.98 ± 0.02	100
MTSΔ1-4	0.31 ± 0.02	31
MTSΔ1-8	0.08 ± 0.01	8.4
MTSΔ1-12	<0.01	< 0.1
MTSΔ1-16	<0.01	< 0.1
R2A	0.47 ± 0.01	48
R3A	1.03 ± 0.06	105
R6A	2.42 ± 0.06	248
R10A	1.41 ± 0.02	144
R2A/R3A/ R6A/R10A	1.10 ± 0.01	113
L11D	2.04 ± 0.01	148
L11D/L13D	0.04 ± 0.01	4
L11D/L13D/ L14D	<0.01	< 0.1

FIGURE 3: Deletion and site-directed mutagenesis of the hPARG59 REG/MTS. The REG/MTS deletion and site-directed mutants are shown in relation to wild-type hPARG59. The exon structure is indicated at the top left. The REG/MTS residues present in each deletion mutant and those mutated by site-directed mutagenesis are also noted. Basic residues of the REG/MTS are indicated with a plus sign (+), and those that are hydrophobic are underlined. To the right, the specific activity and percent activity of each fragment are listed, with the latter being expressed as a percentage of the wild-type hPARG59 value. Data are shown as means of values from two separate experiments, each performed in triplicate.

they point to the vicinal hydrophobic residues L13 and L14 as residues crucial for PARG activity. We have termed this region of PARG the "regulatory segment/MTS" (REG/MTS).

Loss of PARG Activity Is Not Due to Incorrect Protein Folding. CD spectroscopy was performed to determine whether the differences in catalytic activity between hPARG59 and inactive fragments and mutants were due to protein unfolding. Inactive constructs chosen for CD analysis were hPARG42 (consisting of domains C and D), hPARG23 (consisting of domain C only), Δ1−16 (lacking the REG/MTS), and mutant L11D/L13D/L14D. Comparisons of the CD spectra and the mean residue ellipticity values at 222 nm are shown in panels A and B of Figure 4, respectively. hPARG59 exhibited double minima at 208 and 222 nm, consistent with those observed for canonical α-helices. Any protein unfolding, therefore, would be expected to increase the amount of random coil present in the population, and the minima at 222 and 208 nm on the CD spectra would become shallower and move to lower wavelengths, respectively. The deletion of domain B from hPARG59 (fragment hPARG42) resulted in a 2% decrease in helicity. However, the overall molecular population remained mostly α-helical. Domain C alone (hPARG23), on the other hand, showed a much larger decrease in the helical content of ~10%, and the spectrum showed a greater overall β-sheet content as supported by a weaker CD signal, the formation of a single minimum in the 210−220 nm region, and a significant lowering of the maxima at 200 nm. Surprisingly, the deletion of the REG/MTS (Δ1−16) resulted in an increase in helicity. This was unexpected because of the α-helical nature of most MTS (*36*, *37*) and suggests a different secondary structure for this sequence in PARG. Lastly, the mutation of the three hydrophobic leucine residues of the REG/MTS (mutant L11D/L13D/L14D) caused no detectable changes in the conformation of the protein. In addition to excluding loss of secondary structure as the cause of loss of enzymatic activity by deletion or mutation of the REG/MTS, these results provide insight into the molecular composition of the different PARG domains, whose structures still remain to be determined.

Prediction of hPARG59 Secondary Structure. Because of the lack of a crystal structure of PARG, our current knowledge of the molecular folding of the different putative PARG domains is limited. To complement the CD data obtained, secondary structure predictions were made using the PHD and $PROF_{sec}$ algorithms as described in Materials and Methods. Figure 5 shows the prediction models for human PARP-1 (amino acids 664−1014), human PARP-2 (amino acids 233−583), and hPARG59 (amino acids 461−976). The corresponding crystal structures of human PARP-1 and PARP-2 (Protein Data Bank entries 2RCW and 3KJD, respectively) were included to validate the accuracy of the prediction algorithm. The prediction of PARP-1 and PARP-2 secondary structures very closely matches their crystal structures, with a mostly α-helical N-terminal domain followed by a mixed α/β catalytic ADP-ribosyltransferase (ADPRT) domain. β-Sheet 5 (labeled by a red square) in the ADPRT domain contains the catalytic E988 and E534 residues of PARP-1 and PARP-2, respectively. These similarities highlight the potential for these algorithms to relate secondary structure predictions to functional aspects. Catalytic domain C of PARG predicts a secondary structure very similar to that of the PARP-1 and PARP-2 ADPRT domains, which contains a mixture of six β-sheets and three α-helices, and with the localization of the catalytic E756 and E757 residues

A

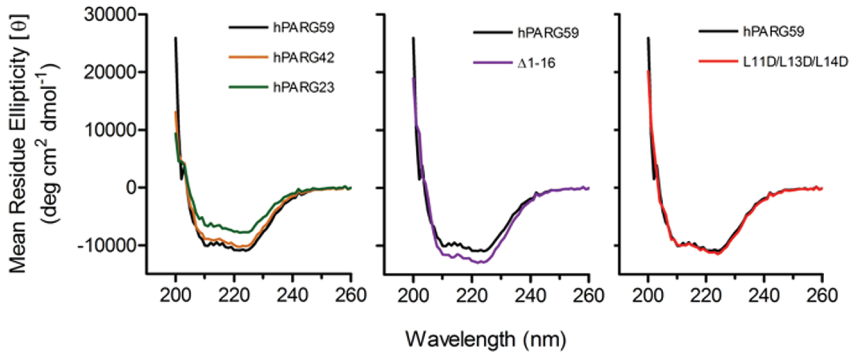

B

Protein	Molecular weight (Daltons)	$[\theta]_{222}$ (deg cm^2 dmol^{-1})	Helicity (%)
hPARG59	102415	-10903	43.7
hPARG42	84941	-10278	41.6
hPARG23	66228	-7833	33.6
Δ1-16	100380	-12943	50.4
L11D/L13D/L14D	102420	-11181	44.6

FIGURE 4: Circular dichroism spectra. (A) The spectra of fragments hPARG42 (brown) and hPARG23 (green) and mutants Δ1−16 (purple) and L11D/L13D/L14D (red) are compared to that of wild-type hPARG59 (black). (B) The molecular weight, mean residue ellipticity at 222 nm, $[\theta]_{222}$, and helical fraction of hPARG42, hPARG23, Δ1−16, and L11D/L13D/L14D are compared to those of wild-type hPARG59.

in β-sheet 5 as seen for PARP-1 and PARP-2. The high incidence of β-sheets in the catalytic domain of PARG emphasizes their major catalytic role in PAR catabolism. Furthermore, domain D is predicted to contain a mostly α-helical region similar to the domains on the N-terminal side of the PARP-1 and PARP-2 ADPRT domains. Hence, on the basis of these secondary structure predictions, the ADPRT-like domain C and the mostly α-helical domain D of PARG strongly resemble those of PARP-1 and PARP-2, with the sole difference being their relative orientation. Such findings can be rationalized by the similarity shared between the substrates of the two classes of enzymes, namely, the ADPR moiety.

Domain B of PARG, on the other hand, is predicted to contain a mixture of random coils, α-helices, and β-sheets. The N-terminal region that includes the REG/MTS is predicted to contain random coils followed by two vicinal β-sheets and four consecutive C-terminal α-helices. A more detailed analysis of the REG/MTS was conducted using the Sub_{sec} algorithm, a subset of $PROF_{sec}$ that predicts the secondary structure of residues that exhibit an average accuracy of >82% (Figure 6A). The REG/MTS was predicted to be in a loop conformation, which was not affected by the L11D, L13D, and L14D mutations. The high probability of hPARG59 to be imported into the mitochondria, as predicted by the MitoProtII computational method (*35*), however, was greatly reduced by the L11D, L13D, and L14D mutations (Figure 6B). In addition, the mutations prevented the detection of a mitochondrial processing peptidase (MPP) cleavage site. These predictions are in agreement with previously reported results showing a 75% reduction in the level of mitochondrial import of the mutant compared to wild-type hPARG59 (*12*). The disruption of the hydrophobicity of the REG/MTS, therefore, affects not only the mitochondrial localization of hPARG59 but also its enzymatic activity. However, this loss of activity is not accompanied by any large change in secondary structure.

The REG/MTS Is Also a Critical Factor in the Catalytic Activity of Full-Length hPARG111. The role of the newly identified regulatory segment in the hPARG59 mitochondrial isoform was investigated in the full-length nuclear hPARG111 protein to determine whether this region could also regulate the enzymatic activity of larger PARG isoforms. While in hPARG59 the regulatory segment corresponds to the N-terminal MTS, in hPARG111 it is an internal region composed of amino acids 461−476 (Figure 1). The REG/MTS was deleted from hPARG111 by site-directed mutagenesis as described in Materials and Methods. As expected, hPARG111 was found to be active, with a specific activity comparable to that of hPARG59 (Figure 7). The hPARG111Δ461−476 deletion mutant, however, exhibited no detectable enzymatic activity, indicating that hPARG111, and consequently also the extranuclear hPARG102 and hPARG99 isoforms, also possess this mechanism of regulation.

DISCUSSION

The study presented here was initiated to identify the minimal catalytic domain of PARG. The identification of an inhibitor-binding site (*18*), three essential catalytic residues (*19*), and a functional glycine-rich region (*20*) all within the putative domain C of PARG pointed to this highly conserved region as the putative minimal catalytic domain. Surprisingly, the smallest active fragment was found to be a 59 kDa fragment, also recently identified as a PARG mitochondrial isoform with an N-terminal MTS required for targeting to the mitochondrial matrix (*11*, *12*). Deletion studies and site-directed mutagenesis of the 16-residue MTS have identified this region, in particular the vicinal hydrophobic leucine residues L13 and L14, as being required for PARG activity (Figure 3), revealing that the residues within the MTS are involved in the regulation of PARG.

The deletion of the REG/MTS from hPARG59 led to an increase in the α-helical content of the protein, which was surprising because the positively charged, amphipathic MTS segments of many proteins are typically predicted to form an α-helix (*11*). In contrast, secondary structure analyses in the study reported

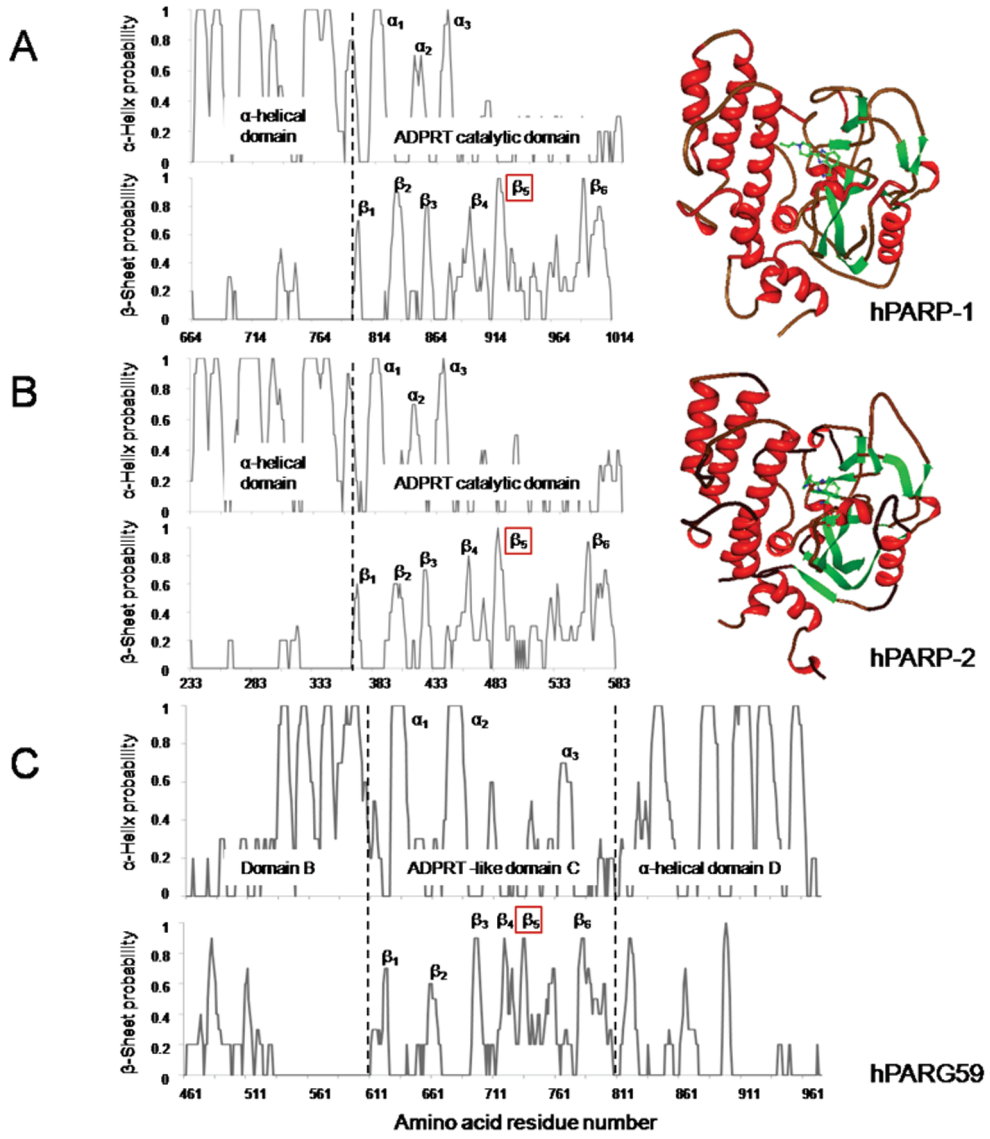

FIGURE 5: Secondary structure predictions. Secondary structure predictions for the mostly α-helical domain and mixed α/*β* ADPRT catalytic domain of hPARP-1 (A) and hPARP-2 (B) are shown adjacent to their respective crystal structures (Protein Data Bank entries 2RCW and 3KJD for hPARP-1 and hPARP-2, respectively) and are compared to that of hPARG59 (C). The ADPRT catalytic domain of PARP-1 and PARP-2 and ADPRT-like catalytic domain C of PARG are aligned to show structural similarity. The α-helices and *β*-sheets are indicated, and *β*-sheet 5, containing the catalytic glutamate residues of each enzyme, is labeled with a red square. The predictions were conducted using the PHD and $PROF_{sec}$ algorithms as described in Materials and Methods.

here using the $PROF_{sec}$ and SUB_{sec} algorithms predicted the REG/MTS to be in a loop conformation (Figure 6A). This prediction is in agreement with the CD data (Figure 4) because the deletion of this loop would be predicted to lower the random coil contribution to the spectrum and increase the α-helical fraction of the protein. Furthermore, a loop conformation would explain the lack of a detectable secondary structure change induced by the L11D, L13D, and L14D mutations in the C-terminal hydrophobic half of the MTS. While amphiphilic properties are not limited to proteins having an α-helical MTS, and considerable flexibility exists in the structural requirements for MTS (*38*), another possibility could be that the formation of an α-helical structure is a downstream event induced by the interaction of hPARG59 with the binding site or cleft of its respective mitochondrial import receptor.

Our data support a model in which the hydrophobic leucine residues of the REG/MTS interact with hydrophobic residues near the catalytic site to activate PARG. Such a model is likely to apply to larger PARG isoforms across different cell compartments, since the deletion of the REG/MTS from full-length hPARG111 also abrogated its catalytic activity. Indeed, the REG/MTS segment is present in all other isoforms of PARG that have been detected to date (*10*, *11*). This raises the possibility that interactions of the REG/MTS with other proteins may generally be involved in PARG regulation. The interplay of PARP-1 and PARG in nuclear PAR metabolism makes automodified PARP-1 a likely candidate for regulation of PARG activity at the REG/MTS site following DNA damage.

The presence of a regulatory segment within the PARG MTS is particularly interesting in that the mechanism of mitochondrial import of proteins with an N-terminal MTS typically involves MTS cleavage by a MPP either during or after entry into the mitochondria (*39*, *40*). This fate of mitochondrial PARG is supported by the detection of an MPP cleavage site by the MitoProtII computational method (Figure 6B). This raises the possibility that interaction with other proteins would be required for

activity of mitochondrial PARG. Recent studies have provided evidence of a mitochondrial localization of PARP-1, dependent on the presence of the mitochondrial protein Mitofilin, with which it interacts and which is poly(ADP-ribosyl)ated upon overactivation of PARP-1 by traumatic brain injury (*41*), although the presence of PARP-1 in the mitochondrial compartment has not yet been validated in cells derived from PARP-1 deficient animals.

While the mechanism of PARG regulation via this segment of PARG needs further investigation, it should be noted that a regulatory domain of PARP-1 involved in protein−protein interactions capable of modulating PARP-1 activation and crucial for its DNA-dependent stimulation has recently been identified (*23*). This domain was found to contain four highly conserved cysteine residues with spacing reminiscent of the zinc finger protein fold and was hence characterized as the third zinc-binding domain of PARP-1. Although the PARG regulatory segment contains only a single cysteine residue and does not have any detectable zinc-binding recognition signatures, it shares the same ability as PARP-1 in regulating catalytic activity from a location very distant from the active site (>250 residues). A comparison of six PARG sequences across a wide range of organisms revealed a high level of homology in the REG/MTS (Figure 8). Particular attention was given to the level of conservation of basic and hydrophobic residues, which was found to be high. Indeed, L14 is invariant across these organisms. The strong sequence homology provides further support for the notion that this region of PARG is involved in the regulation of PARG activity.

A look at the secondary structure predictions of hPARG59, in concert with the CD data, provides evidence of a mixed α/β domain C and a mostly α-helical domain D, which are very similar to the catalytic ADPRT domain and the mostly α-helical domain, respectively, of PARP-1 and PARP-2. The only significant difference lies in the orientation of the two domains. These predicted structural similarities between the active sites are due to the similar compositions of their substrates, namely, the ADPR moiety, and are further supported by the cross inhibition of PARG inhibitors with PARP-1 observed with several PARG inhibitors currently being developed in our laboratory (unpublished data). While this potential for cross inhibition may prove to have therapeutic benefits, particularly in the new paradigm of cancer therapy based on synthetic sickness/lethality (SSL), which has paved the way for the clinical development of PARP inhibitors in breast tumors with germline mutations in BRCA1 and/or BRCA2 (*42*, *43*), it also poses difficulties in obtaining specific PARG inhibitors. This newly identified regulatory segment of PARG, therefore, offers a potentially novel site for drug targeting that could be exploited for the development of specific and potent PARG inhibitors to serve as tools in the validation of PARG as a therapeutic target.

A

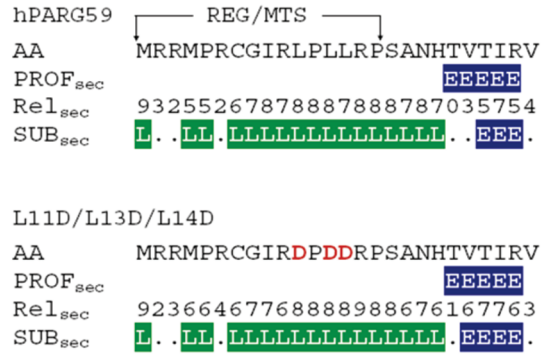

B

Protein	Export to mitochondria probability	Mitochondrial fraction (%)	Cleavage site
hPARG59	0.97	95	P^{16}
L11D/L13D/L14D	0.63	20	ND

FIGURE 6: PARG REG/MTS is predicted to be in a loop conformation. (A) PROF$_{sec}$ secondary structure predictions of wild-type REG/MTS and the L11D/L13D/L14D mutant. The three mutated residues are colored red. Abbreviations: AA, amino acid; L, loop; E, β-sheet; Rel$_{sec}$, reliability index for PROF$_{sec}$ prediction (0 for low to 9 for high); SUB$_{sec}$, subset of the PROF$_{sec}$ algorithm for all residues with an expected average accuracy of >82%. (B) Predicted and observed changes in REG/MTS function induced by the L11D/L13D/L14D mutant. The export to mitochondria probabilities and cleavage site detections were obtained using the MitoProtII computational method (*35*), while the mitochondrial fraction values have been previously reported (*12*).

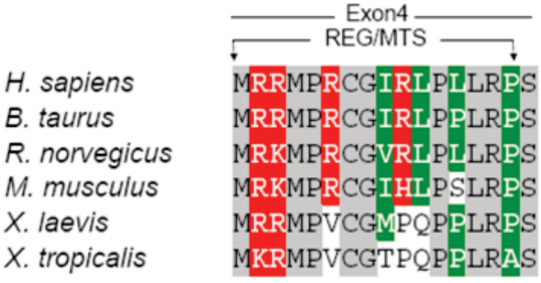

FIGURE 8: Comparison of PARG amino acid sequences from different species. The amino acid sequence of the REG/MTS encoded by exon 4 was aligned with five additional PARG sequences across a wide range of organisms. Residues colored gray represent sequence identity in all six organisms, while those colored red and green represent conservation of basic and hydrophobic residues, respectively. The GenBank accession numbers for PARG are as follows: Q86W56 for *Homo sapiens*, O02776 for *Bacillus taurus*, Q9QYM2 for *Rattus norvegicus*, O88622 for *Mus musculus*, Q4KLP9 for *Xenopus laevis*, and B1H3J2 for *Xenopus tropicalis*.

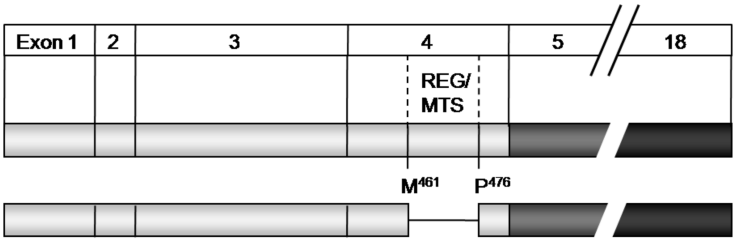

Protein	Specific Activity (nmol/min/mg)	Activity (%)
hPARG111	1.02 ± 0.03	100
hPARG111 Δ461-476	<0.01	<0.1

FIGURE 7: Deletion of the REG/MTS from full-length hPARG111. Deletion mutagenesis was used to characterize the role of the REG/MTS in the enzymatic activity of the full-length hPARG111 protein. The REG/MTS and its first and last amino acid residues are indicated. The specific activities and percent activities are shown as means of values from two separate experiments, each performed in triplicate.

ACKNOWLEDGMENT

DNA sequence analyses were performed by the University of Arizona Genetic Analysis and Technology Core Service Facility. All circular dichroism experiments were performed at the University of Arizona Analytical Biophysics Core Facility run by Dr. Chad K. Park.

REFERENCES

1. Juarez-Salinas, H., Sims, J. L., and Jacobson, M. K. (1979) Poly-(ADP-ribose) levels in carcinogen-treated cells. *Nature 282*, 740–741.
2. Schreiber, V., Dantzer, F., Ame, J. C., and de Murcia, G. (2006) Poly(ADP-ribose): Novel functions for an old molecule. *Nat. Rev. Mol. Cell Biol. 7*, 517–528.
3. Heeres, J. T., and Hergenrother, P. J. (2007) Poly(ADP-ribose) makes a date with death. *Curr. Opin. Chem. Biol. 11*, 644–653.
4. Kleine, H., Poreba, E., Lesniewicz, K., Hassa, P. O., Hottiger, M. O., Litchfield, D. W., Shilton, B. H., and Luscher, B. (2008) Substrate-assisted catalysis by PARP10 limits its activity to mono-ADP-ribosylation. *Mol. Cell 32*, 57–69.
5. Hottiger, M. O., Hassa, P. O., Luscher, B., Schuler, H., and Koch-Nolte, F. (2010) Toward a unified nomenclature for mammalian ADP-ribosyltransferases. *Trends Biochem. Sci. 35*, 208–219.
6. Lindahl, T., Satoh, M. S., Poirier, G. G., and Klungland, A. (1995) Post-translational modification of poly(ADP-ribose) polymerase induced by DNA strand breaks. *Trends Biochem. Sci. 20*, 405–411.
7. Miwa, M., Tanaka, M., Matsushima, T., and Sugimura, T. (1974) Purification and properties of glycohydrolase from calf thymus splitting ribose-ribose linkages of poly(adenosine diphosphate ribose). *J. Biol. Chem. 249*, 3475–3482.
8. Lin, W., Ame, J. C., Aboul-Ela, N., Jacobson, E. L., and Jacobson, M. K. (1997) Isolation and characterization of the cDNA encoding bovine poly(ADP-ribose) glycohydrolase. *J. Biol. Chem. 272*, 11895–11901.
9. Oka, S., Kato, J., and Moss, J. (2006) Identification and characterization of a mammalian 39-kDa poly(ADP-ribose) glycohydrolase. *J. Biol. Chem. 281*, 705–713.
10. Meyer-Ficca, M. L., Meyer, R. G., Coyle, D. L., Jacobson, E. L., and Jacobson, M. K. (2004) Human poly(ADP-ribose) glycohydrolase is expressed in alternative splice variants yielding isoforms that localize to different cell compartments. *Exp. Cell Res. 297*, 521–532.
11. Meyer, R. G., Meyer-Ficca, M. L., Whatcott, C. J., Jacobson, E. L., and Jacobson, M. K. (2007) Two small enzyme isoforms mediate mammalian mitochondrial poly(ADP-ribose) glycohydrolase (PARG) activity. *Exp. Cell Res. 313*, 2920–2936.
12. Whatcott, C. J., Meyer-Ficca, M. L., Meyer, R. G., and Jacobson, M. K. (2009) A specific isoform of poly(ADP-ribose) glycohydrolase is targeted to the mitochondrial matrix by a N-terminal mitochondrial targeting sequence. *Exp. Cell Res. 315*, 3477–3485.
13. Koh, D. W., Lawler, A. M., Poitras, M. F., Sasaki, M., Wattler, S., Nehls, M. C., Stoger, T., Poirier, G. G., Dawson, V. L., and Dawson, T. M. (2004) Failure to degrade poly(ADP-ribose) causes increased sensitivity to cytotoxicity and early embryonic lethality. *Proc. Natl. Acad. Sci. U.S.A. 101*, 17699–17704.
14. Hanai, S., Kanai, M., Ohashi, S., Okamoto, K., Yamada, M., Takahashi, H., and Miwa, M. (2004) Loss of poly(ADP-ribose) glycohydrolase causes progressive neurodegeneration in *Drosophila melanogaster*. *Proc. Natl. Acad. Sci. U.S.A. 101*, 82–86.
15. Cortes, U., Tong, W. M., Coyle, D. L., Meyer-Ficca, M. L., Meyer, R. G., Petrilli, V., Herceg, Z., Jacobson, E. L., Jacobson, M. K., and Wang, Z. Q. (2004) Depletion of the 110-kilodalton isoform of poly(ADP-ribose) glycohydrolase increases sensitivity to genotoxic and endotoxic stress in mice. *Mol. Cell. Biol. 24*, 7163–7178.
16. El-Khamisy, S. F., Masutani, M., Suzuki, H., and Caldecott, K. W. (2003) A requirement for PARP-1 for the assembly or stability of XRCC1 nuclear foci at sites of oxidative DNA damage. *Nucleic Acids Res. 31*, 5526–5533.
17. Gao, H., Coyle, D. L., Meyer-Ficca, M. L., Meyer, R. G., Jacobson, E. L., Wang, Z. Q., and Jacobson, M. K. (2007) Altered poly(ADP-ribose) metabolism impairs cellular responses to genotoxic stress in a hypomorphic mutant of poly(ADP-ribose) glycohydrolase. *Exp. Cell Res. 313*, 984–996.
18. Koh, D. W., Patel, C. N., Ramsinghani, S., Slama, J. T., Oliveira, M. A., and Jacobson, M. K. (2003) Identification of an inhibitor binding site of poly(ADP-ribose) glycohydrolase. *Biochemistry 42*, 4855–4863.
19. Patel, C. N., Koh, D. W., Jacobson, M. K., and Oliveira, M. A. (2005) Identification of three critical acidic residues of poly(ADP-ribose) glycohydrolase involved in catalysis: Determining the PARG catalytic domain. *Biochem. J. 388*, 493–500.
20. Panda, S., Poirier, G. G., and Kay, S. A. (2002) tej defines a role for poly(ADP-ribosyl)ation in establishing period length of the *Arabidopsis* circadian oscillator. *Dev. Cell 3*, 51–61.
21. Oliveira, M. A., Koh, D. W., Patel, C. N., and Jacobson, M. K. (2001) Structure-based characterization of a novel anticancer target poly-(ADP-ribose) glycohydrolase (PARG): Evidence for the presence of an ADP-ribosyltransferase (ADPRT) fold. *Proc. Am. Assoc. Cancer Res. 42*, 832.
22. Rolli, V., Ruf, A., Augustin, A., Schulz, G. E., Ménissier-de Murcia, J., and de Murcia, G. (2000) in From DNA Damage and Stree Signaling to Cell Death: Poly ADP-ribosylation Reactions (de Murcia, G., and Shall, S., Eds.) Oxford University Press, New York.
23. Langelier, M. F., Servent, K. M., Rogers, E. E., and Pascal, J. M. (2008) A third zinc-binding domain of human poly(ADP-ribose) polymerase-1 coordinates DNA-dependent enzyme activation. *J. Biol. Chem. 283*, 4105–4114.
24. Langelier, M. F., Ruhl, D. D., Planck, J. L., Kraus, W. L., and Pascal, J. M. (2010) The Zn3 domain of human poly(ADP-ribose) polymerase-1 (PARP-1) functions in both DNA-dependent poly(ADP-ribose) synthesis activity and chromatin compaction. *J. Biol. Chem. 285*, 18877–18887.
25. Kauppinen, T. M., Chan, W. Y., Suh, S. W., Wiggins, A. K., Huang, E. J., and Swanson, R. A. (2006) Direct phosphorylation and regulation of poly(ADP-ribose) polymerase-1 by extracellular signal-regulated kinases 1/2. *Proc. Natl. Acad. Sci. U.S.A. 103*, 7136–7141.
26. Cohen-Armon, M., Visochek, L., Rozensal, D., Kalal, A., Geistrikh, I., Klein, R., Bendetz-Nezer, S., Yao, Z., and Seger, R. (2007) DNA-independent PARP-1 activation by phosphorylated ERK2 increases Elk1 activity: A link to histone acetylation. *Mol. Cell 25*, 297–308.
27. Hassa, P. O., Haenni, S. S., Buerki, C., Meier, N. I., Lane, W. S., Owen, H., Gersbach, M., Imhof, R., and Hottiger, M. O. (2005) Acetylation of poly(ADP-ribose) polymerase-1 by p300/CREB-binding protein regulates coactivation of NF-κB-dependent transcription. *J. Biol. Chem. 280*, 40450–40464.
28. Menard, L., and Poirier, G. G. (1987) Rapid assay of poly(ADP-ribose) glycohydrolase. *Biochem. Cell Biol. 65*, 668–673.
29. Myers, J. K., Pace, C. N., and Scholtz, J. M. (1997) Helix propensities are identical in proteins and peptides. *Biochemistry 36*, 10923–10929.
30. Chen, Y. H., and Yang, J. T. (1971) A new approach to the calculation of secondary structures of globular proteins by optical rotatory dispersion and circular dichroism. *Biochem. Biophys. Res. Commun. 44*, 1285–1291.
31. Rost, B., Yachdav, G., and Liu, J. (2004) The PredictProtein server. *Nucleic Acids Res. 32*, W321–W326.
32. Rost, B. (1996) PHD: Predicting one-dimensional protein structure by profile-based neural networks. *Methods Enzymol. 266*, 525–539.
33. Rost, B., and Sander, C. (1993) Prediction of protein secondary structure at better than 70% accuracy. *J. Mol. Biol. 232*, 584–599.
34. Rost, B. (2001) Review: Protein secondary structure prediction continues to rise. *J. Struct. Biol. 134*, 204–218.
35. Claros, M. G., and Vincens, P. (1996) Computational method to predict mitochondrially imported proteins and their targeting sequences. *Eur. J. Biochem. 241*, 779–786.
36. von Heijne, G. (1986) Mitochondrial targeting sequences may form amphiphilic helices. *EMBO J. 5*, 1335–1342.
37. Lemire, B. D., Fankhauser, C., Baker, A., and Schatz, G. (1989) The mitochondrial targeting function of randomly generated peptide sequences correlates with predicted helical amphiphilicity. *J. Biol. Chem. 264*, 20206–20215.
38. Roise, D., Theiler, F., Horvath, S. J., Tomich, J. M., Richards, J. H., Allison, D. S., and Schatz, G. (1988) Amphiphilicity is essential for mitochondrial presequence function. *EMBO J. 7*, 649–653.
39. Lithgow, T. (2000) Targeting of proteins to mitochondria. *FEBS Lett. 476*, 22–26.
40. Koehler, C. M. (2000) Protein translocation pathways of the mitochondrion. *FEBS Lett. 476*, 27–31.
41. Lai, Y., Chen, Y., Watkins, S. C., Nathaniel, P. D., Guo, F., Kochanek, P. M., Jenkins, L. W., Szabo, C., and Clark, R. S. (2008) Identification of poly-ADP-ribosylated mitochondrial proteins after traumatic brain injury. *J. Neurochem. 104*, 1700–1711.
42. Fong, P. C., Boss, D. S., Yap, T. A., Tutt, A., Wu, P., Mergui-Roelvink, M., Mortimer, P., Swaisland, H., Lau, A., O'Connor, M. J., Ashworth, A., Carmichael, J., Kaye, S. B., Schellens, J. H., and de Bono, J. S. (2009) Inhibition of poly(ADP-ribose) polymerase in tumors from BRCA mutation carriers. *N. Engl. J. Med. 361*, 123–134.
43. Amir, E., Seruga, B., Serrano, R., and Ocana, A. (2010) Targeting DNA repair in breast cancer: A clinical and translational update. *Cancer Treat. Rev.* (in press).